

Electrical control of near-field energy transfer between quantum dots and 2D semiconductors

Dhiraj Prasai[†], Andrey R. Klots[#], AKM Newaz^{#§}, J. Scott Niezgoda[‡], Noah J. Orfield[‡], Carlos A. Escobar[§], Alex Wynn[#], Anatoly Efimov^{||}, G. Kane Jennings[§], Sandra J. Rosenthal^{†‡¶↓}, Kirill I. Bolotin^{#}*

[†]Interdisciplinary Graduate Program in Materials Science, Vanderbilt University, Nashville TN, USA [#]Department of Physics and Astronomy, Vanderbilt University, Nashville TN, USA [§]Department of Physics and Astronomy, San Francisco State University, San Francisco CA, USA [‡]Department of Chemistry, Vanderbilt University, Nashville TN, USA [§]Department of Chemical and Biomolecular Engineering, Nashville TN, USA ^{||}Center for Integrated Nanotechnologies, Los Alamos National Laboratory, Los Alamos NM, USA [¶]Vanderbilt Institute for Nanoscale Science and Engineering, Nashville TN, USA [↓]Materials Science and Technology Division, Oak Ridge National Laboratory, Oak Ridge TN, USA.

ABSTRACT: We investigate near-field energy transfer between chemically synthesized quantum dots (QDs) and two-dimensional semiconductors. We fabricate devices in which electrostatically gated semiconducting monolayer molybdenum disulfide (MoS₂) is placed atop a homogenous self-assembled layer of core-shell CdSSe QDs. We demonstrate efficient non-radiative Förster resonant energy transfer (FRET) from QDs into MoS₂ and prove that modest gate-induced variation in the excitonic absorption of MoS₂ lead to large (~500%) changes in the FRET rate. This, in turn, allows for up to ~75% electrical modulation of QD photoluminescence intensity. The hybrid QD/MoS₂ devices operate within a small voltage range, allow for continuous modification of the QD photoluminescence intensity, and can be used for selective tuning of QDs emitting in the visible-IR range.

KEYWORDS: Quantum Dots, MoS₂, TMDCs, FRET, electrical modulation.

Introduction

Nanoscale optical emitters – such as semiconductor quantum dots (QDs) or fluorophores - are strongly affected by their environment. An optical excitation in a nanoemitter can be transferred into the environment non-radiatively via processes

such as charge transfer and Förster resonant energy transfer (FRET). Among these processes, FRET is a uniquely efficient long-range optical process.¹ Electrical control of FRET is desirable for potential applications of nanoemitters. To enable such control, materials with optical properties that respond

to electric field are required. Recently discovered two-dimensional materials, such as graphene or MoS₂ are ideal for this purpose. Due to their atomic thickness, optical parameters of these materials can be controlled via electrostatic gating.²⁻⁵ We therefore expect that by placing a nanoemitter onto a 2D material, it may be possible to electrically control the FRET pathway between the two systems.

Here, we explore FRET between chemically synthesized QDs and two-dimensional semiconductor (2DSC) monolayer molybdenum disulfide (MoS₂).^{6, 7} FRET in such a system is especially interesting due to the presence of tightly bound excitons in MoS₂ that are stable at room temperature.⁸⁻¹¹ Moreover, the oscillator strength of these excitons is strongly modified by the presence of the charge carriers in MoS₂.²⁻⁴ We find strong quenching of photoluminescence (PL) for QDs near MoS₂, demonstrate that this quenching is due to FRET between QDs and excitons in MoS₂, and prove that other mechanisms such as charge transfer do not play a role in this system. Furthermore, we observe ~75% modulation of QD photoluminescence intensity with electrostatic gating of MoS₂. We find that this phenomenon is caused by ~500% electrical modulation of the QD/MoS₂ FRET rate. This, in turn, is due to changes in the near-field absorption of MoS₂ related to interaction of MoS₂ excitons with free charge carriers.

Very recently, related approaches have been demonstrated to achieve electrical control of the FRET rate for QDs and other nanoscale infrared emitters near another 2D

material, graphene.^{12, 13} Our use of 2DSC offers several distinct advantages. The sizeable bandgaps of 2DSCs allow us to achieve electrical modulation of FRET from QDs emitting in the visible range. The strong electrical modulation of excitons in 2DSCs allows for the operation of devices with significantly reduced electrical fields, compared to graphene. Finally, we show selective modulation of QDs at desired wavelengths by choosing 2DSCs with corresponding excitonic features.¹⁴

FRET between QDs and two-dimensional semiconductors

To explore near-field energy transfer between QDs and 2DSCs, it is important to understand the conditions under which this type of transfer is expected. In general, FRET between two systems depends on their separation distance and the overlap integral between the absorption and emission spectra. The Fermi golden rule yields the following estimate for the FRET rate between a 0D and

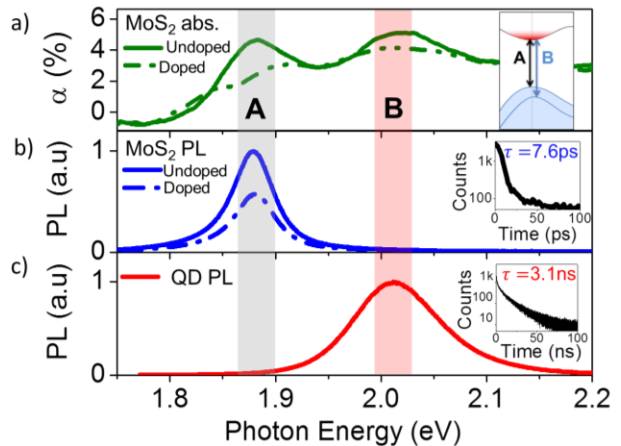


Figure 1 (a) Absorption spectra of monolayer MoS₂ at two different doping levels. Inset: bandstructure of MoS₂ near its K-point. (b) PL spectra of monolayer MoS₂ at two different doping levels. Inset: time-resolved PL due to A-excitons in MoS₂. (c) PL spectrum of CdSSe QDs. Inset: time-resolved PL of excitons in QDs.

a 2D system (details in Supporting Information, S1):^{1, 15, 16}

$$k_{FRET} \sim \frac{1}{d^4} \int_0^\infty \alpha(\lambda) f(\lambda) \lambda^4 d\lambda. \quad (1)$$

In this expression $f(\lambda)$ is the normalized emission of QDs, $\alpha(\lambda)$ is the absorption coefficient for a 2DSC as a function of wavelength λ , and d is the distance between QDs and a 2DSC. The peculiar d^4 dependence of k_{FRET} is a characteristic of near-field coupling between excitations in 0D and 2D systems.^{1, 16} Equation (1) indicates that in order to observe large k_{FRET} , the following conditions must be satisfied: (i) The optical absorption of the 2DSC must be sizable at the QD emission wavelength. (ii) A QD/2DSC separation d must be small. (iii) The lifetime of an exciton in QDs, τ_{QD} , must be longer than the inverse rate of energy transfer, k_{FRET}^{-1} . When this condition is fulfilled, an exciton in a QD lives long enough to transfer its energy into a 2DSC.

We can now select the appropriate materials to observe and explore FRET between QDs and 2DSCs. From the diverse group of 2DSCs (*e.g.*: MoS₂, WSe₂, WS₂), we

chose monolayer MoS₂, a direct band gap semiconductor that is well studied, readily available, and optically active in the visible range.^{6, 7} The absorption spectrum of MoS₂ (Fig. 1a) is dominated by two strong excitonic PL peaks at 1.88eV (A) and 2.05eV (B). These features are due to absorption of light by tightly bound band-edge A- and B-excitons⁸⁻¹¹ residing at the K-point of the Brillouin zone (Fig 1a, inset). The energy separation between the excitons is due to strong spin-orbit interaction¹¹ that splits the valence band of MoS₂. The photoluminescence spectrum of MoS₂ is dominated by A-excitons, the lowest excited state (Fig. 1b). With increased electron doping, both absorption (Fig. 1a, dashed line) and photoluminescence (Fig. 1b, dashed line) of MoS₂ are strongly reduced for energies corresponding to A- and B-peaks. This strong electro-optical effect is related to the interaction between excitons and free charge carriers in MoS₂. Doping-induced reduction of absorption is attributed to a combination of phase-space filling effect (blocking of low-momentum states that are needed for exciton formation) and screening of electron-hole interactions by free carriers.^{17, 18} Additionally, doping allows the formation of charged

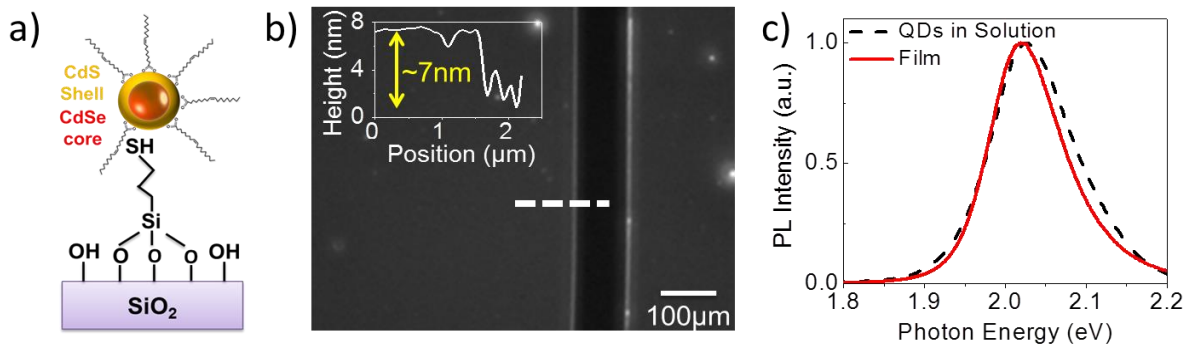


Figure 2 (a) CdSe QDs with oleic acid ligands attached to functionalized SiO₂. (b) PL image of a QD film. A striation made on the film is evident as a dark strip. Inset: AFM height profile of the film obtained along the white dashed line in (b). (c) Normalized PL spectra of a QD film on SiO₂ and of the same QDs in solution.

excitons (trions),^{3, 4} that become the new lowest-energy excitonic state and hence modify the PL spectrum.

We chose compositionally graded alloy core-shell CdSSe QDs¹⁹ as the emission source. The QDs were synthesized to emit at $\sim 2.02\text{eV}$ (Fig. 1c), very close to the B-peak in the absorption spectrum of MoS₂ (Fig. 1a). Additionally, CdSSe QDs are bright (quantum yield $\sim 50\%$) and have lifetimes $\sim 3\text{ns}$ (Fig. 1c, Inset). This is much longer than the $\sim 8\text{ps}$ lifetime of excitons in MoS₂ (Fig. 1b, Inset; see “Methods” for measurement details). This ensures that FRET will be directed from QDs to MoS₂.^{20, 21} Due to the spectral separation between the PL peaks of QDs and MoS₂, their spectra can be analyzed independently in hybrid structures.

Having spectrally satisfied FRET conditions in our hybrid structures, the next step is to physically bring QDs and a 2DSC in close proximity. We developed a flexible approach to address the biggest challenge in such devices – fabrication of uniform

monolayer films of QDs. First, we used chemical self-assembly to deposit a uniform layer of QDs onto a SiO₂ substrate. The SiO₂ substrate functionalized with (3-Mercaptopropyl) trimethoxysilane was submerged into a solution of oleic acid-ligated CdSSe QDs (Fig 2a, see “Methods” for details).²² The exposed thiol groups displace the oleic acid surface ligands and bind the QDs to the substrate.²³ The density of QDs was optimized to produce sub-monolayer films such that PL peaks due to QDs and MoS₂ could be distinguished. We used PL spectroscopy and atomic force microscopy (AFM) to assess the uniformity of QD films. With AFM we determined that the thickness of the QD film is $\sim 7\text{nm}$ (Fig. 2b, Inset). This thickness is consistent with a sub-monolayer film of QDs that are $\sim 5\text{nm}$ in diameter and have 1-2nm long oleic acid ligands.²⁴ Photoluminescence imaging indicates that as-fabricated QD films remain bright and are very uniform (Fig. 2b). Moreover, the position and the width of the PL peak for the QD film (Fig 2c, red line) do

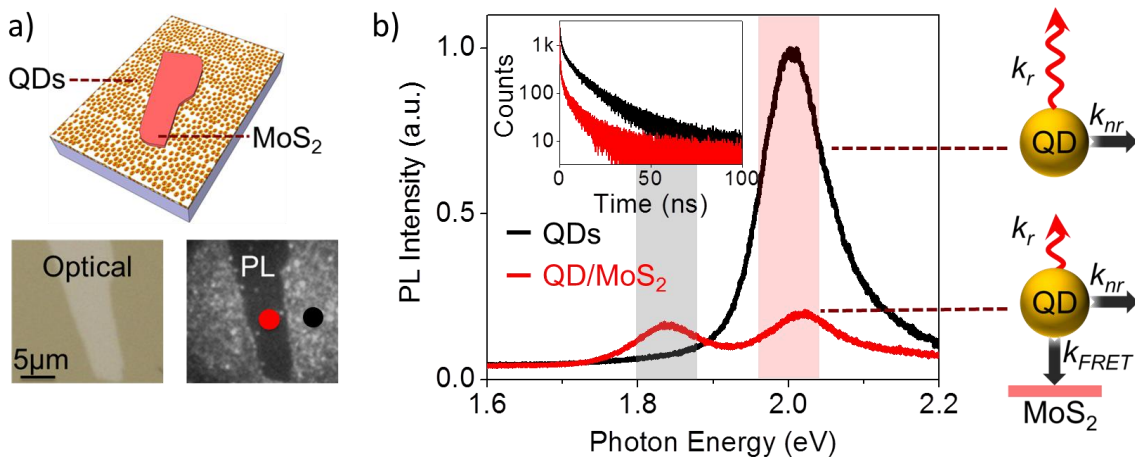


Figure 3 (a) Ungated MoS₂/QD device along with its optical (left) and photoluminescence (right) images. PL image was recorded using a band-pass filter (605nm-615nm) only transmitting QD emission. (b) PL spectra and time-resolved PL (Inset) of QD/MoS₂ hybrid (red) and of bare QD film (black). The spectra were recorded from the same device shown in Fig. 3a at positions marked by red and black circles. The schematic on the right illustrates FRET between a QD and MoS₂.

not differ significantly from that of same QDs in solution (Fig 2c, black dotted line). This suggests that the QDs are not chemically modified during the process of self-assembly and that the interactions between QDs are negligible. Each QD in the film can therefore be treated as a single emitter.

Finally, we mechanically transferred a monolayer MoS₂ onto QDs using fabrication techniques developed for 2D heterostructures.^{25, 26} Several experimental tests described below confirm that such transfer does not perturb the QD layer.

Results and Discussion

Experimental evidence of FRET

A typical sample along with its optical and PL image is shown in Fig. 3a. This sample can be considered ungated ($V_g=0$) compared to electrostatically gated devices studied further. Both the PL image and PL spectra (Fig. 3a,b) indicate strong suppression of photoluminescence for the QDs that are close to MoS₂. To quantify this effect, we introduce the quenching factor $Q = I_{QD}/I_{QD/MoS_2}$. Here I_{QD/MoS_2} is the height of the QD photoluminescence peak at 2.02eV for the hybrid QD/MoS₂ device (acquired at a point marked red in Fig. 3a), and I_{QD} is the height of the same peak from QDs away from MoS₂ (acquired at a point marked black in Fig. 3a). We calculate $Q(0V)\sim 4.8$ from the data shown in Fig. 3b. We also observed that the lifetimes of QDs reduce by a similar amount due to the presence of MoS₂, $\tau_{QD}/\tau_{QD/MoS_2}\sim 4.4$ (Fig. 3b, Inset). At the same time, the position of the PL peak due to QDs remained virtually unchanged at about ~ 2.02 eV (Fig. 3b). This indicates that the QDs are not

chemically or mechanically perturbed by MoS₂.

The quenched PL and decreased lifetimes indicate the opening of an additional non-radiative relaxation channel for the QDs next to MoS₂. We attribute this pathway to FRET. Strong spectral overlap between the emission spectrum of QDs and B-peak in absorption of MoS₂ coupled with very small QD/MoS₂ separation should, according to Eq. (1), lead to large k_{FRET} . Prior experiments on similar QDs next to 2D systems (graphene, MoS₂) arrived at a similar conclusion.^{27, 28}

We confirmed that mechanisms other than FRET are not responsible for observed changes in PL in our devices. In principle, charge transfer between QDs and MoS₂ can also lead to non-radiative relaxation.²⁹⁻³¹ For our experiments we intentionally chose core-shell QDs with strong electron-hole pair confinement and long ligands.²⁴ Charge transfer in such core-shell QDs is likely inefficient or absent.³² To further exclude the contribution of charge transfer, we fabricated devices with a spacer layer (5-15nm of SiO₂) inserted between QDs and MoS₂. Despite large MoS₂/QD separation, we observed significant quenching in PL of QDs atop of MoS₂ (Supporting Information, S2). Such quenching can only be attributed to long-range FRET, as short-range charge transfer should be fully suppressed in spacer devices.³³ In addition, charge transfer is conclusively ruled by the optoelectronic measurements described in the last section of the manuscript. It is also feasible that dielectric screening due to MoS₂ could affect the intensity of QD photoluminescence. To exclude this possibility, we fabricated devices

where hBN, an optically transparent insulator, is transferred onto QDs instead of MoS₂ (Supporting Information, S3). While hBN has a dielectric constant $\epsilon \sim 4-7$,³⁴ similar to that of monolayer MoS₂,³⁵ we did not observe any spectral changes or quenching for QDs in hBN/QD devices. This confirms that the QDs are not affected by dielectric screening due to neighboring materials. This also rules out the possibility of mechanical or chemical changes to the QD layer during the transfer procedure.

The QD/MoS₂ FRET rate was estimated from measured suppression of QD photoluminescence and lifetimes. The intensity of QD photoluminescence depends on radiative (k_r) and non-radiative (k_{nr}, k_{FRET}) decay rates:

$$I_{QD} \sim \frac{k_r}{k_r + k_{nr}} = k_r \tau_{QD},$$

$$I_{QD/MoS_2} \sim \frac{k_r}{k_r + k_{nr} + k_{FRET}} = k_r \tau_{QD/MoS_2} \quad (2)$$

In these equations, the lifetime of a QD is expressed as an inverse of the sum of radiative and non-radiative rates, and k_r is assumed to be unaffected by the environment. Equation (2) confirms that near-equal suppression of QD lifetime and PL intensity observed in our experiments is an expected consequence of FRET. From the measured PL quenching $Q \sim 4.8$, using equation (2) we determined $k_{FRET} = (Q - 1)/\tau_{QD} \sim (1.1 \pm 0.2) \times 10^9 \text{ s}^{-1}$. Importantly, this rate corresponds to lifetime $\sim 1 \text{ ns}$, shorter than the intrinsic QD lifetime of $\sim 3 \text{ ns}$. From measured Q and assuming separation distance between QD-core and MoS₂ $\sim 3.5 \text{ nm}$ (Fig 2b, inset), we evaluate FRET radius $R_0 \sim 5 \text{ nm}$.

Electrical modulation of FRET

Finally, we examined gate-induced modification of the optical properties of QD/MoS₂ devices. To enable such a study, we used fabrication described previously, but with MoS₂ transferred on top of pre-patterned gold electrodes. An optically transparent solid electrolyte was then deposited onto MoS₂ (Fig. 4a, see ‘‘Methods’’ for details). This configuration allows us to vary the carrier density inside MoS₂ while being able to perform optical measurements. It is also important to note that electric field is near-absent at the location of QDs and cannot affect their photoluminescence directly.³⁶ Although very high carrier densities, $n \sim 10^{14} \text{ cm}^{-2}$, can be reached with electrolyte gates (Supporting Information, S4),³⁷ our devices require much smaller densities, $n \sim 10^{13} \text{ cm}^{-2}$, and efficiently operate at low gate voltages ($-2 \text{ V} < V_g < 2 \text{ V}$). Overall, we fabricated and measured 4 devices including the representative device shown in Fig. 4a.

With increased electron doping (positive V_g), we observed a well-known suppression of the PL peak^{2, 3} due to MoS₂ at 1.88eV as discussed earlier (Fig. 1b and Supporting Information Fig. S4b). On the other hand, photoluminescence of QDs at $\sim 2.02 \text{ eV}$ strongly increases with V_g (Fig. 4b). In our best device, we observed up to $\sim 75\%$ modulation of the QD photoluminescence intensity for V_g between -2 V and 2 V . This effect is reproducible for all measured devices and is stable over multiple sweeps of V_g (Fig. 4b, Inset).

We attribute the modulation of PL to gate-induced modulation of the FRET rate k_{FRET} . Indeed, as discussed above, optical absorption

$\alpha(\lambda)$ of MoS₂ is strongly changing with V_g at 2.05eV, the energy corresponding to QD emission (Fig. 1c). According to the equation (1), changes in $\alpha(\lambda)$ should lead to modulation of the FRET rate, and hence QD

PL intensity.

Our next goal is to understand the relationship between FRET modulation and MoS₂ absorption. In a separate measurement on a device without a QD layer, we used

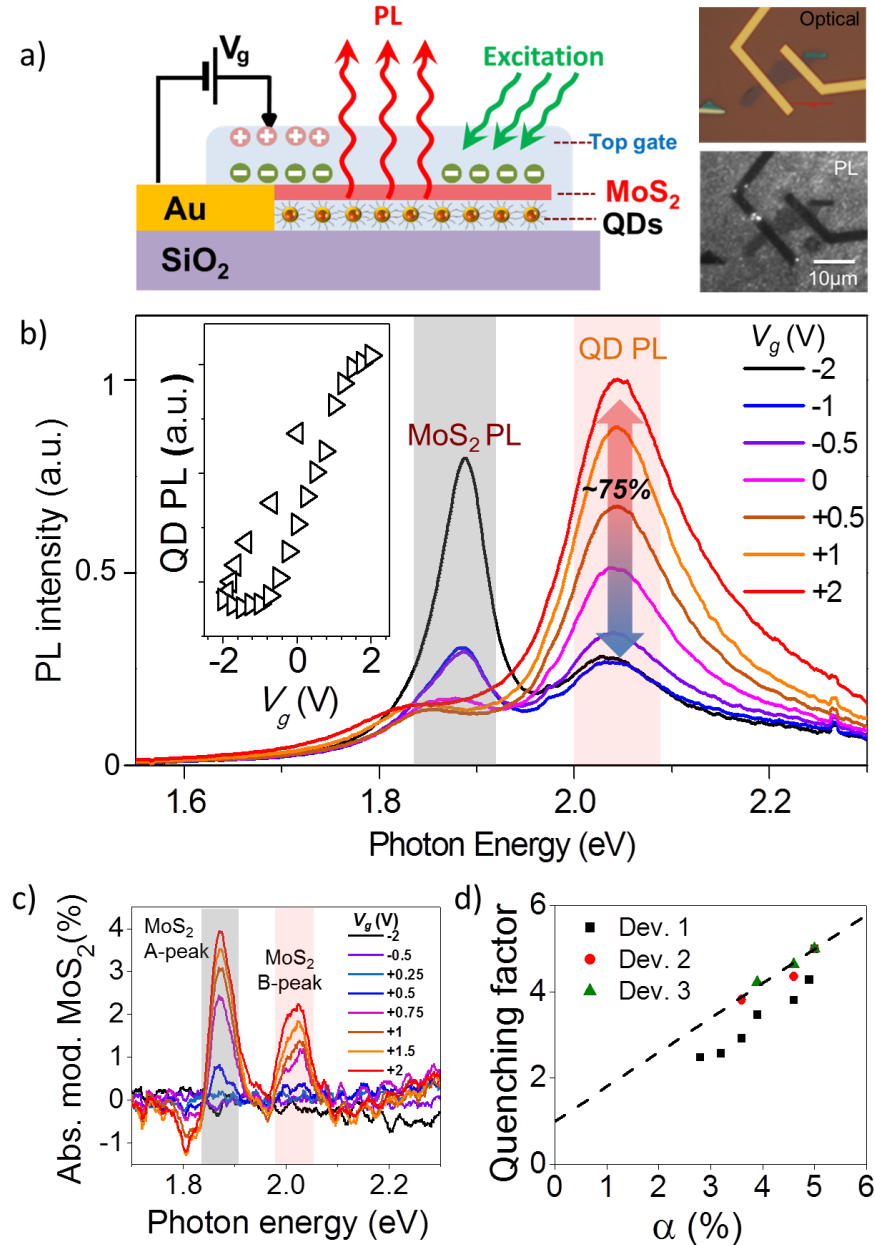


Figure 4 (a) Device schematic of electrolyte gated QD/MoS₂ hybrid. Optical and photoluminescence images of an electrically contacted QD/MoS₂ device. (b) PL spectra of a QD/MoS₂ device at different V_g . Inset: QD photoluminescence intensity vs. V_g during a back-and-forth sweep between +2V and -2V. (c) Transmittance modulation of MoS₂. The dip at ~1.8eV is likely related to charged exciton absorption. (d) From the measured Q vs. V_g from (a) and α vs. V_g from (b), a single parametric $Q(\alpha)$ plot was created. Since the transmission of MoS₂ is only reliably determined for $V_g > 0$, only these points were used in the plot (details in Supporting Information, S6).

confocal transmission microscopy to record gate-induced transmittance modulation of MoS₂ defined as

$$M = (I(\hbar\omega, V_g) - I(\hbar\omega, 0V)) / I(\hbar\omega, 0V).$$

Here $I(\hbar\omega, V_g)$ is the intensity of light transmitted through MoS₂ at photon energy $\hbar\omega$ and gate voltage V_g . We use transmittance modulation as a proxy measurement for far-field absorption which is otherwise hard to assess via conventional differential reflectivity measurements for our device geometry. A simple estimate yields $\alpha(V_g) = \alpha(V_g = 0V) - M(V_g)$ (Details in Methods and Supporting Information, S5). Within our gating range we observe only $\sim 2\%$ modulation of MoS₂ transmittance at $\sim 2.05\text{eV}$ (Fig. 4c), much smaller than $\sim 75\%$ modulation in QD photoluminescence.

We devised a simple model relating near-field FRET rate and quenching factor to far-field absorption of MoS₂. The normalized emission spectrum of an individual QD centered at wavelength λ is narrow compared to the relatively broad absorption features of MoS₂.³⁸ In this situation, equation (1) can be simplified to

$$k_{FRET} \sim \frac{1}{d^4} \alpha(\lambda, V_g).$$

Combining this with equation (2), we obtain the following expression for the quenching factor Q :

$$\begin{aligned} Q(\lambda, V_g) &= \frac{\tau_{QD}}{\tau_{QD/MoS_2}} = 1 + \tau_{QD} k_{FRET} \\ &= 1 + A\alpha(\lambda, V_g). \end{aligned} \quad (3)$$

Here $A \sim \frac{\tau_{QD}}{d^4}$ is a proportionality constant relating the quenching factor to absorption of MoS₂. From experimentally measured $Q(V_g=0) \sim 5$ (Fig. 3b) and $\alpha(V_g=0) \sim 5\%$ (Fig. 1b) at $\lambda=610\text{nm}$ (QD emission peak), we find $A = (Q(0) - 1)/\alpha(0) \sim 80$. The large value of A translates to large electrical modulation of PL of the QDs. To check the validity of our model, we plotted experimentally acquired values of Q and α . The measured $Q(\alpha)$ along with the prediction of equation (3) (dashed line) are plotted in Fig. 4d. The agreement between the experimental data and our model confirms that the observed modulation of QD photoluminescence is a consequence of electrical modulation of FRET. From Fig. 4b (inset) and equation (3) we also find that the FRET rate changes from $2.8 \times 10^9\text{s}^{-1}$ to $0.5 \times 10^9\text{s}^{-1}$ within our gating range.

We devised additional control experiments to further confirm that the observed PL modulation is related to gate-induced changes in excitonic absorption of two-dimensional semiconductors and not to other mechanisms. We fabricated one device where MoS₂ is substituted by a monolayer of graphene and another QD/MoS₂ device with different CdSSe QDs emitting at $\sim 2.2\text{eV}$, not in resonance with MoS₂ absorption peaks. In contrast to the devices discussed above (e.g. in Fig. 4), in both of these samples optical absorption of the 2D material is gate-independent at the QD emission wavelength (Fig. 4c and Supporting Information, S7). As expected, since FRET modulation is spectrally selective, we did not observe any gate-dependent changes of the QD photoluminescence in either device in the

range of gate voltage between -3V and 3V. Finally, we fabricated a device with QDs emitting at $\sim 2.4\text{eV}$, but with a different 2DSC, WS_2 , instead of MoS_2 . Large and clear modulation of QD PL is observed in this device since the gate-dependent excitonic peaks of WS_2 (A-peak: 2.0eV , B-peak: 2.4eV)³⁹ are in resonance with the QD emission peak (Supporting Information, S8).

These observations confirm that PL of QDs is only affected by the absorbance of a 2D material at relevant frequencies and not just its carrier density. We therefore strengthen our claim that charge transfer between MoS_2 and QDs is either absent or does not depend on gate voltage. The lack of PL modulation in QD/graphene devices further highlights the advantage of 2DSCs for modulation of QDs in the visible (as opposed to IR^{12, 13}) range. Furthermore, we see that QD/2DSC hybrids can be used for selective modulation of QDs emitting at different wavelengths.

In summary, we demonstrated electrical control of the near-field energy transfer between QDs and two-dimensional semiconductors (MoS_2 , WS_2). We found that it is related to modulation of excitonic absorption of 2D semiconductors, and achieved $\sim 75\%$ modulation of QD photoluminescence in the visible range. It is instructive to compare our approach to other existing schemes to control photoluminescence of QDs via electrical signals. Some of the existing schemes utilize electrochemical injection of charge carriers into QDs,^{30, 31} electron-hole dissociation under applied electric fields,⁴⁰ or controlled Stark shifts.⁴¹ In all of these schemes, electrical fields are applied directly to the

QDs. In our approach the electric field changes the parameters of a two-dimensional semiconductor and is absent at the location of QDs.³⁶ We do not expect electrochemical modification of QDs. The operating principle of our scheme – electrical control over the QD/2DSC FRET rate – can be extended to other nanoemitters. Finally, QDs emitting at different wavelengths over the visible and IR ranges can be modulated by choosing two-dimensional semiconductors with varied bandgaps (e.g.: WSe_2 , WS_2 , MoSe_2).

We envision several potential improvements in our system. FRET efficiency, and hence the efficiency of PL modulation, can be increased by reducing the distance between QDs and 2DSCs (equations (1) and (3)). This can be achieved by either reducing QD shell-size or by shortening QD ligands. Additionally, 2DSCs could be gated more efficiently using ultrathin gate dielectrics. The advances in CVD growth^{42, 43} of 2DSCs could lead to inexpensive fabrication of large-scale QD/2DSC hybrids. Overall, QD/2DSC hybrids could be used as efficient and electrically tunable light sources operating anywhere in the visible to IR spectral range. Potential applications for such devices range from solid-state lighting and high-resolution passive (“e-ink”) displays to biosensors.

Methods

Synthesis of $\text{CdS}_x\text{Se}_{1-x}$ Graded Alloy Quantum Dots. This one-pot synthetic procedure is based on a method published recently by Harrison *et al.*¹⁹ First, 1 mmol CdO (0.128 g), 1.3 mL oleic acid (HOA), and 20 mL 1-octadecene (ODE) were heated to 100°C under vacuum for 10 minutes, and

subsequently purged with Ar. The temperature was increased to 260°C and the conversion of red CdO to colorless Cd-oleate was monitored to completion, after which the reaction temperature was reduced to 220°C. Solutions of S:Tributyl phosphate (0.75 M) and Se:Tributyl phosphate (0.75 M) in ODE were prepared separately and 0.8 mL aliquots of each were pulled into the same syringe. The S/Se aliquot was swiftly injected into the Cd-oleate flask at 220°C and the reaction was allowed to proceed for 2hrs. The nanocrystals were cooled and precipitated with a 3:1 mixture of butanol and ethanol, resuspended in toluene, and precipitated twice more with pure ethanol. After being finally suspended in toluene, the nanocrystals were passed through a 0.45µm filter and stored.

QD/MoS₂ device fabrication. Cr/Au (2nm/30nm) electrodes were deposited on SiO₂ substrates. The substrates were then cleaned in a piranha solution (1:3 H₂O₂:H₂SO₄) for 1 hour, made hydrophilic through O₂ plasma treatment (30s), and functionalized in 1mM solution of (3-Mercaptopropyl) trimethoxysilane in hexane for 10 min. Functionalized substrates were washed in a hexane bath for 1 min, rinsed in isopropanol, and blow-dried. To assemble a uniform film of QDs, functionalized substrates were placed into 5mg/ml solution of CdSSe for 30mins and rinsed gently afterwards with toluene. To transfer MoS₂ onto QDs, we followed the recipe developed by Zomer et al.²⁶ We spun Elvacite polymer (~1µm thick) onto PDMS/clear Scotch tape sandwich structure. The structure was baked at 90°C for 5mins. Monolayer MoS₂ was exfoliated onto Elvacite and verified using optical microscopy and Raman spectroscopy.

MoS₂ was aligned with Au electrodes, brought into contact with QD films and baked at 120°C. The PDMS/polymer layer was then mechanically separated from the MoS₂/QD stack. To remove the polymer residues, the MoS₂/QD stack was soaked in acetone for 15 min. Finally, we created the solid electrolyte gate by placing a drop of CsClO₄ salt in poly(ethylene) oxide (PEO) matrix dissolved in acetonitrile and drying it for 2hrs at room temperature. A second gate electrode close to MoS₂ was used to contact the solid electrolyte.

PL measurements. PL spectra were recorded at ambient conditions using a Thermo Scientific DXR Raman microscope with a 100µW, 532nm (~2.3eV) laser as an excitation source. MoS₂ was electrically gated using a Keithley 2400 sourcemeter connected to the solid electrolyte. PL modulation of MoS₂ was used to confirm gating efficiency. PL images were collected using a conventional fluorescence microscopy setup with a 605-615nm bandpass filter and green light (530–590 nm) excitation.

Time resolved PL measurements. PL lifetimes of QDs were recorded using a modified version of a home-built confocal microscope described previously.⁴⁴ A 400 nm pulsed beam with a repetition rate of 250kHz was reflected from a 410nm long-pass dichroic filter (Omega Optics 3RD410LP) and focused through a water immersion objective to a confocal spot on the QD layer of the fabricated devices. PL was collected through the objective and subsequently passed through the dichroic filter and a 610 ± 5nm bandpass filter to select for QD PL. The QD photoluminescence was then focused onto the array of a single photon avalanche

diode (Micro Photon Devices PDM series SPAD). Lifetime data was collected in the form of single photon events *via* a time correlated single photon counting (TCSPC) correlator (PicoHarp 300) with a time resolution of 4ps. Time-resolved PL from MoS₂ was measured using a grating spectrometer (Acton) coupled to a streak camera system (Hamamatsu). The second harmonic of a femtosecond Ti:sapphire laser with 450 nm pump pulses, 100fs in duration was used for excitation. Two-dimensional spectrograms were acquired in photon-counting mode with 2nm spectral resolution and a minimum 3ps temporal resolution. Time-resolved PL spectra were fitted by a tri-exponential function and lifetimes were estimated as weighted averages of three decay rates.

Absorption/transmittance modulation measurements. Standard differential reflectivity measurements could not be performed on our samples due to the non-uniformity of the solid electrolyte layer. Instead, we used confocal transmission microscopy to determine absorbance/transmittance of gated MoS₂ devices on transparent glass substrates. A broad (~1mm) light beam from a fiber-coupled halogen light source was used to illuminate our sample. Light passed through the sample was collected through a 40X objective and was further magnified ~10 times and focused on a screen with a ~0.5mm diameter pinhole. The pinhole blocks the light from the rest of the sample while transmitting light that passes through MoS₂. The spectrum

of the transmitted light as a function of gate voltage was recorded using Shamrock 303i spectrometer. We note that due to the low quantum yield of MoS₂,⁶ its PL cannot interfere with our absorption measurements. Differential transmittance measurements of MoS₂ devices on glass without the solid electrolyte layer (Fig. 1b) were obtained using the same technique.

Supporting Information

Qualitative discussion of 0D/2D FRET. PL measurement of MoS₂/Spacer/QD devices. PL Measurement of QD/hBN devices. Measurements of carrier density *vs.* V_g for a graphene Hall-bar device gated using solid electrolyte. PL spectra *vs.* V_g for a MoS₂ device gated using solid electrolyte. Detailed discussion and schematic of optical transmittance measurements. Detailed description of $Q(\alpha)$ measurements. PL spectra *vs.* V_g for control QD/graphene and QD/MoS₂ devices. PL spectra *vs.* V_g for green QD/WS₂, green QD/MoS₂ and red QD/MoS₂

Corresponding Author

*Email: kirill.bolotin@vanderbilt.edu

Acknowledgements

We acknowledge useful discussions with Kirill Velizhanin. The work was primarily supported by the Office of Naval Research award N000141310299 with additional funding from NSF EPS-1004083, NSF CBET-1134509 and NSF DMR-1056859.

References

1. Swathi, R. S.; Sebastian, K. L. *J. Chem. Phys.* **2009**, 130, 086101.
2. Newaz, A. K. M.; Prasai, D.; Ziegler, J. I.; Caudel, D.; Robinson, S.; Haglund Jr, R. F.; Bolotin, K. I. *Sol. Stat. Comm.* **2013**, 155, 49-52.
3. Mak, K. F.; He, K.; Lee, C.; Lee, G. H.; Hone, J.; Heinz, T. F.; Shan, J. *Nat. Mater.* **2013**, 12, 207-211.
4. Ross, J. S.; Wu, S.; Yu, H.; Ghimire, N. J.; Jones, A. M.; Aivazian, G.; Yan, J.; Mandrus, D. G.; Xiao, D.; Yao, W.; Xu, X. *Nat. Commun.* **2013**, 4, 1474.
5. Wang, F.; Zhang, Y.; Tian, C.; Girit, C.; Zettl, A.; Crommie, M.; Shen, Y. R. *Science* **2008**, 320, 206-209.
6. Mak, K.; Lee, C.; Hone, J.; Shan, J.; Heinz, T. *Phys. Rev. Lett.* **2010**, 105, 136805.
7. Splendiani, A.; Sun, L.; Zhang, Y.; Li, T.; Kim, J.; Chim, C.-Y.; Galli, G.; Wang, F. *Nano. Lett.* **2010**, 10, 1271-1275.
8. Klots, A. R.; Newaz, A. K. M.; Wang, B.; Prasai, D.; Krzyzanowska, H.; Lin, J.; Caudel, D.; Ghimire, N. J.; Yan, J.; Ivanov, B. L.; Velizhanin, K. A.; Burger, A.; Mandrus, D. G.; Tolk, N. H.; Pantelides, S. T.; Bolotin, K. I. *Sci. Rep.* **2014**, 4, 6608.
9. Chernikov, A.; Berkelbach, T. C.; Hill, H. M.; Rigosi, A.; Li, Y.; Aslan, O. B.; Reichman, D. R.; Hybertsen, M. S.; Heinz, T. F. *Phys. Rev. Lett.* **2014**, 113, 076802.
10. Ye, Z.; Cao, T.; O'Brien, K.; Zhu, H.; Yin, X.; Wang, Y.; Louie, S. G.; Zhang, X. *Nature* **2014**, 513, 214-218.
11. Molina-Sánchez, A.; Sangalli, D.; Hummer, K.; Marini, A.; Wirtz, L. *Phys. Rev. B* **2013**, 88, 045412.
12. Lee, J.; Bao, W.; Ju, L.; Schuck, P. J.; Wang, F.; Weber-Bargioni, A. *Nano. Lett.* **2014**, 14, 7115-7119.
13. Tielrooij, K. J.; Orona, L.; Ferrier, A.; Badioli, M.; Navickaite, G.; Coop, S.; Nanot, S.; Kalinic, B.; Cesca, T.; Gaudreau, L.; Ma, Q.; Centeno, A.; Pesquera, A.; Zurutuza, A.; de Riedmatten, H.; Goldner, P.; Garcia de Abajo, F. J.; Jarillo-Herrero, P.; Koppens, F. H. L. *Nat. Phys.* **2015**, DOI: 10.1038/nphys3204.
14. Xia, F.; Wang, H.; Xiao, D.; Dubey, M.; Ramasubramaniam, A. *Nat. Photon.* **2014**, 8, 899-907.
15. Clegg, R. M., Chapter 1 Förster resonance energy transfer—FRET what is it, why do it, and how it's done. In *Laboratory Techniques in Biochemistry and Molecular Biology*, Gadella, T. W. J., Ed. Elsevier: 2009; Vol. 33, pp 1-57.
16. Federspiel, F.; Froehlicher, G.; Nasilowski, M.; Pedetti, S.; Mahmood, A.; Doudin, B.; Park, S.; Lee, J.-O.; Halley, D.; Dubertret, B.; Gilliot, P.; Berciaud, S. *Nano. Lett.* **2015**, DOI: 10.1021/nl5044192.
17. Zhang, C.; Wang, H.; Chan, W.; Manolatou, C.; Rana, F. *Phys. Rev. B* **2014**, 89, 205436.
18. Schmitt-Rink, S.; Chemla, D. S.; Miller, D. A. B. *Adv. Phys.* **1989**, 38, 89-188.
19. Harrison, M. A.; Ng, A.; Hmelo, A. B.; Rosenthal, S. J. *Isr. J. Chem.* **2012**, 52, 1063-1072.
20. Hemdana, I.; Mahdouani, M.; Bourguiga, R. *Phys. B: Cond. Matt.* **2012**, 407, 3313-3319.
21. Korn, T.; Heydrich, S.; Hirmer, M.; Schmutzler, J.; Schüller, C. *Appl. Phys. Lett.* **2011**, 99, 102109.
22. Zhu, M.-Q.; Chang, E.; Sun, J.; Drezek, R. A. *J. Mat. Chem.* **2007**, 17, 800-805.
23. Ravindran, S.; Chaudhary, S.; Colburn, B.; Ozkan, M.; Ozkan, C. S. *Nano. Lett.* **2003**, 3, 447-453.
24. Gunawan, A. A.; Chernomordik, B.; Plemmons, D.; Deng, D.; Aydil, E.; Mkhoyan, A. *Microsc. Microanal.* **2013**, 19, 1506-1507.
25. Dean, C. R.; Young, A. F.; MericI; LeeC; WangL; SorgenfreiS; WatanabeK; TaniguchiT; KimP; Shepard, K. L.; HoneJ. *Nat. Nano.* **2010**, 5, 722-726.

26. Zomer, P. J.; Dash, S. P.; Tombros, N.; van Wees, B. J. *Appl. Phys. Lett.* **2011**, *99*, 232104.
27. Chen, Z.; Berciaud, S.; Nuckolls, C.; Heinz, T. F.; Brus, L. E. *ACS Nano* **2010**, *4*, 2964-2968.
28. Prins, F.; Goodman, A. J.; Tisdale, W. A. *Nano. Lett.* **2014**, *14*, 6087-6091.
29. Sharma, S. N.; Pillai, Z. S.; Kamat, P. V. *J. Phys. Chem. B* **2003**, *107*, 10088-10093.
30. Jha, P. P.; Guyot-Sionnest, P. *J. Phys. Chem. C* **2007**, *111*, 15440-15445.
31. Jha, P. P.; Guyot-Sionnest, P. *J. Phys. Chem. C* **2010**, *114*, 21138-21141.
32. Li, S.; Steigerwald, M. L.; Brus, L. E. *ACS Nano* **2009**, *3*, 1267-1273.
33. Paul, A.; Watson, R. M.; Wierzbinski, E.; Davis, K. L.; Sha, A.; Achim, C.; Waldeck, D. H. *J. Phys. Chem. B* **2010**, *114*, 14140-14148.
34. Geick, R.; Perry, C. H.; Rupprecht, G. *Physical Review* **1966**, *146*, 543-547.
35. Chen, X.; Wu, Z.; Xu, S.; Wang, L.; Huang, R.; Han, Y.; Ye, W.; Xiong, W.; Han, T.; Long, G.; Wang, Y.; He, Y.; Cai, Y.; Sheng, P.; Wang, N. *Nat. Commun.* **2015**, *6*.
36. Larentis, S.; Tolsma, J. R.; Fallahazad, B.; Dillen, D. C.; Kim, K.; MacDonald, A. H.; Tutuc, E. *Nano. Lett.* **2014**, *14*, 2039-2045.
37. Efetov, D.; Maher, P.; Glinskis, S.; Kim, P. *Phys. Rev. B* **2011**, *84*, 161412.
38. Empedocles, S.; Norris, D.; Bawendi, M. *Phys. Rev. Lett.* **1996**, *77*, 3873-3876.
39. Zhao, W.; Ghorannevis, Z.; Chu, L.; Toh, M.; Kloc, C.; Tan, P.-H.; Eda, G. *ACS Nano* **2013**, *7*, 791-797.
40. Liu, S.; Borys, N. J.; Huang, J.; Talapin, D. V.; Lupton, J. M. *Phys. Rev. B* **2012**, *86*, 045303.
41. Bennett, A. J.; Patel, R. B.; Skiba-Szymanska, J.; Nicoll, C. A.; Farrer, I.; Ritchie, D. A.; Shields, A. J. *Appl. Phys. Lett.* **2010**, *97*, 031104.
42. van der Zande, A. M.; Huang, P. Y.; Chenet, D. A.; Berkelbach, T. C.; You, Y.; Lee, G.-H.; Heinz, T. F.; Reichman, D. R.; Muller, D. A.; Hone, J. C. *Nat. Mater.* **2013**, *12*, 554-561.
43. Lee, Y.-H.; Zhang, X.-Q.; Zhang, W.; Chang, M.-T.; Lin, C.-T.; Chang, K.-D.; Yu, Y.-C.; Wang, J. T.-W.; Chang, C.-S.; Li, L.-J.; Lin, T.-W. *Adv. Mater.* **2012**, *24*, 2320-2325.
44. Orfield, N. J.; McBride, J. R.; Keene, J. D.; Davis, L. M.; Rosenthal, S. J. *ACS Nano* **2015**, *9*, 831-9.

Supporting Information

S1. Supplementary discussion: FRET between 0D and a 2D system

In general, the rate of Forster Resonant Energy Transfer (k_{FRET}) between two quantum dots follows from the Fermi's golden rule and is well-known (Reference 1 of the main manuscript):

$$k_{FRET(0D-0D)} \sim |\vec{E}|^2 \int_0^\infty \varepsilon_A(\lambda) f(\lambda) \lambda^4 d\lambda.$$

Here $|\vec{E}|^2$ is the square of electric field created by a QD dipole at the position of the other QD, $f(\lambda)$ is the normalized emission spectrum of the donor QD as a function of wavelength λ , and $\varepsilon_A(\lambda)$ is the acceptor molar extinction coefficient. Since dipole field decays with distance as r^{-3} , $|\vec{E}|^2$ is proportional to r^{-6} . Therefore, $k_{FRET(0D-0D)}$ has the same distance dependence.

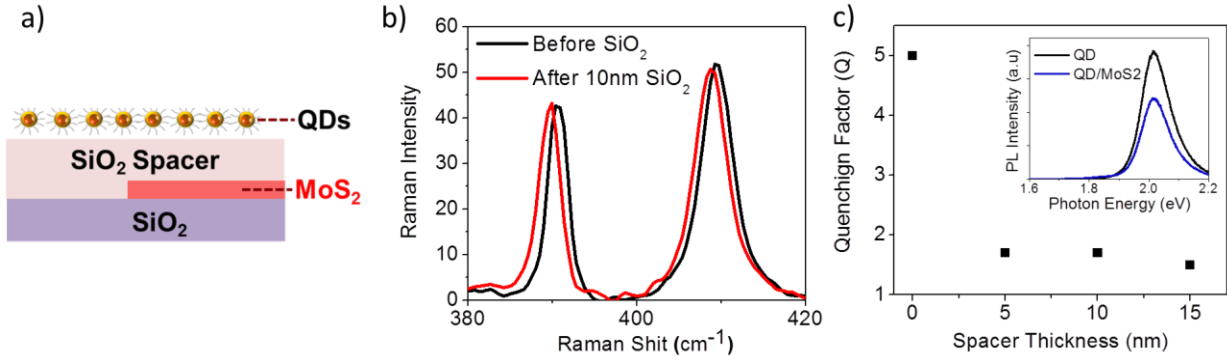
For the case of FRET between a 0D and a 2D system, we can formally split a 2D material into a 2D array of point-like absorbers and then integrate $k_{FRET(0D-0D)}$ over 2D material area. If the 2D material is located in oXY plane and a QD is elevated above that plane by distance d , the distance r between QD and the point on the plane can be written as $r = \sqrt{d^2 + x^2 + y^2}$. Then integration over area yields:

$$k_{FRET(0D-2D)} \sim \int_{Area} d(Area) k_{FRET(0D-0D)} \sim \int_{Area} \frac{dxdy}{\sqrt{d^2 + x^2 + y^2}^6} \int_0^\infty \varepsilon_A(\lambda) f(\lambda) \lambda^4 d\lambda.$$

Replacing absorptivity $\varepsilon_A(\lambda)$ by 2D absorption coefficient $\alpha(\lambda)$ and performing simple integration over area we obtain the expression used in the main text:

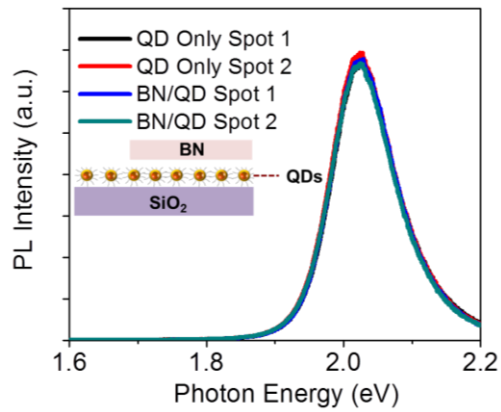
$$k_{FRET} \sim \frac{1}{d^4} \int_0^\infty \alpha(\lambda) f(\lambda) \lambda^4 d\lambda.$$

S2. MoS₂ – Spacer – QD Device



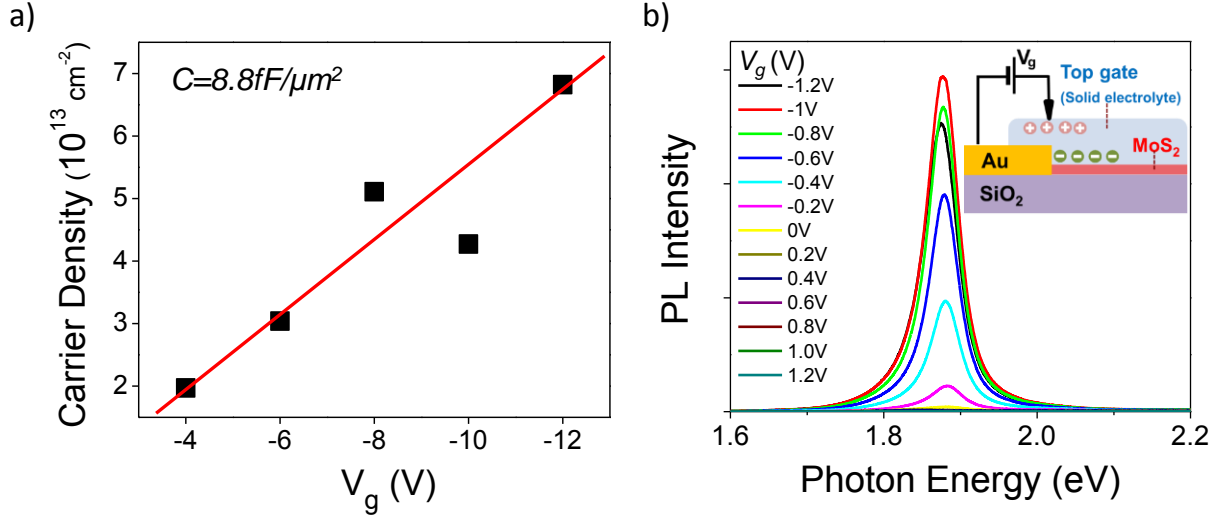
Supplementary Figure S2 (a) Device schematic for MoS₂/spacer/QD device. (b) Raman spectra of MoS₂ before (black) and after (red) SiO₂ spacer deposition. (c) QD quenching factor vs. spacer thickness. Inset: PL spectra of QD and QD/MoS₂ for 15nm spacer device.

S3. hBN – QD Device



Supplementary Figure S3 Photoluminescence spectra for QDs covered by hBN (blue and green curves) and QDs away from hBN (black and red curves). Inset: schematic of a hBN/QD device.

S4. Solid electrolyte characterization



Supplementary Figure S4 (a) The efficiency of the solid electrolyte gating approach was estimated using a separate graphene Hall-bar device covered by the same electrolyte used in QD/MoS₂ devices. Carrier density n vs. gate voltage V_g in that device was determined via Hall measurements. From a fit (red line) to the acquired $n(V_g)$ data (black symbols), we extract an estimate for the capacitance of the polymer electrolyte, $C \sim 8.8 \text{ fF}/\mu\text{m}^2$. **(b)** PL modulation of a representative gated MoS₂ device without the QD layer. Schematic of the device is shown in the inset.

S5. Confocal transmission microscopy

The absorption spectrum of MoS₂ could not be obtained directly from standard differential reflectivity measurements for our electrolyte gated MoS₂ samples. This is due to the non-uniformity of the solid electrolyte layer. Instead, we used confocal transmission microscopy to determine transmittance modulation of gated MoS₂ devices on transparent glass substrates (Fig. S5). Transmittance modulation is defined as $M = \left(I(\hbar\omega, V_g) - I(\hbar\omega, 0V) \right) / I(\hbar\omega, 0V)$, where $I(\hbar\omega, V_g)$ is the intensity of light transmitted through MoS₂ at photon energy $\hbar\omega$ and gate voltage V_g . Transmittance modulation is closely related to absorption modulation. We can rewrite the definition of M as

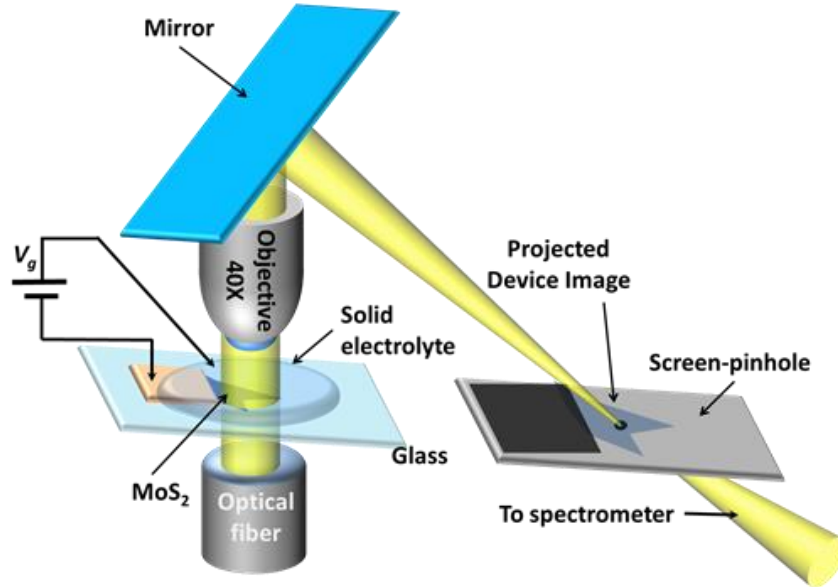
$$M = \frac{\frac{I(\hbar\omega, V_g)}{I_0(\hbar\omega)} - \frac{I(\hbar\omega, 0V)}{I_0(\hbar\omega)}}{\frac{I(\hbar\omega, 0V)}{I_0(\hbar\omega)}}.$$

Here $I_0(\hbar\omega)$ is the intensity of the incident light. Since $I(\hbar\omega, V_g)/I_0(\hbar\omega) = 1 - \alpha(\hbar\omega, V_g)$, we get:

$$M = \frac{\alpha(\hbar\omega, 0V) - \alpha(\hbar\omega, V_g)}{1 - \alpha(\hbar\omega, 0V)}.$$

Since MoS₂ absorption is small (~5%) in our wavelength region, $M \approx \alpha(\hbar\omega, 0V) - \alpha(\hbar\omega, V_g)$ or $\alpha(\hbar\omega, V_g) = \alpha(\hbar\omega, V_g = 0V) - M(\hbar\omega, V_g)$. Therefore, we can estimate $\alpha(\hbar\omega, V_g)$ from measured M and $\alpha(\hbar\omega, V_g = 0V) \sim 5\%$ obtained from an unbiased MoS₂ flake before deposition of solid electrolyte.

Experimentally, a broad (~1mm) light beam from a fiber-coupled halogen light source was used to illuminate our sample. Light passed through the sample was collected through a 40X objective and was further magnified ~10 times and focused on a screen with a ~0.5mm diameter pinhole. A magnified image of the device was projected on the screen. The pinhole was adjusted to block the light from the rest of the sample while transmitting light that passes through MoS₂. The spectrum of the transmitted light as a function of gate voltage was recorded using Shamrock 303i spectrometer.



Supplementary Figure S5 Schematic of measurement set up for transmission microscopy.

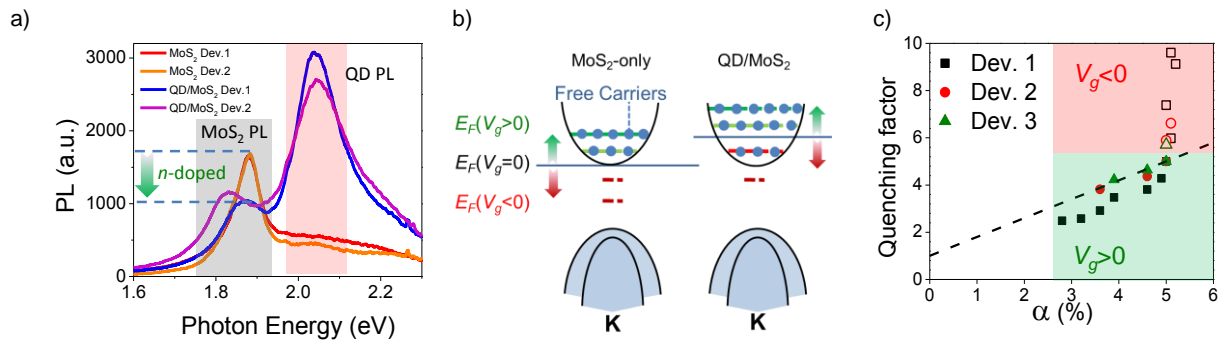
S6. Supplementary Discussion: Detailed description of $Q(\alpha)$ measurement

The data in the $Q(\alpha)$ parametric plot (Fig. 4d, main text) were obtained as follows. A QD/MoS₂ device was used for measurements of the quenching factor Q vs. V_g . However, absorption of the MoS₂ layer, α_{MoS_2} , could not be determined in the same device due to the strong background absorption of the QDs. For that reason, a separate MoS₂-only device without QDs was used for α_{MoS_2} vs. V_g measurements (Fig. 4c of the main text, Supporting information S5). However, interpretation of $Q(\alpha)$ data is complicated by the difference of the intrinsic doping levels of MoS₂ between QD/MoS₂ and MoS₂-only devices. Indeed, at $V_g=0$ we observed reduced PL due to MoS₂ (peak at ~1.9eV) in QD/MoS₂ as compared to MoS₂-only devices (Fig. S4b). Since PL of

MoS₂ can be used as a proxy for free carrier density (Fig. 1b, Fig. S4b, Fig.S6a), this observation suggests that the intrinsic doping level of MoS₂ in MoS₂-only devices is *lower* than that of MoS₂ in QD/MoS₂ devices. Moreover, the observation of near-absent absorption modulation for MoS₂ in MoS₂-only devices for $V_g < 0$ (as compared to strong absorption modulation for $V_g > 0$) suggests that the density of free carriers in that device approaches ~ 0 at $V_g = 0$ (Fig. 4c). In contrast, robust changes of MoS₂ and QD photoluminescence in QD/MoS₂ devices (Fig. 4b, main text) hint that the density of free carriers is changing throughout our gating range and the Fermi level always stays within the conduction band. In Fig.S6b, we illustrated the proposed Fermi level positioning between MoS₂ and QD/MoS₂ devices due to difference in intrinsic doping levels.

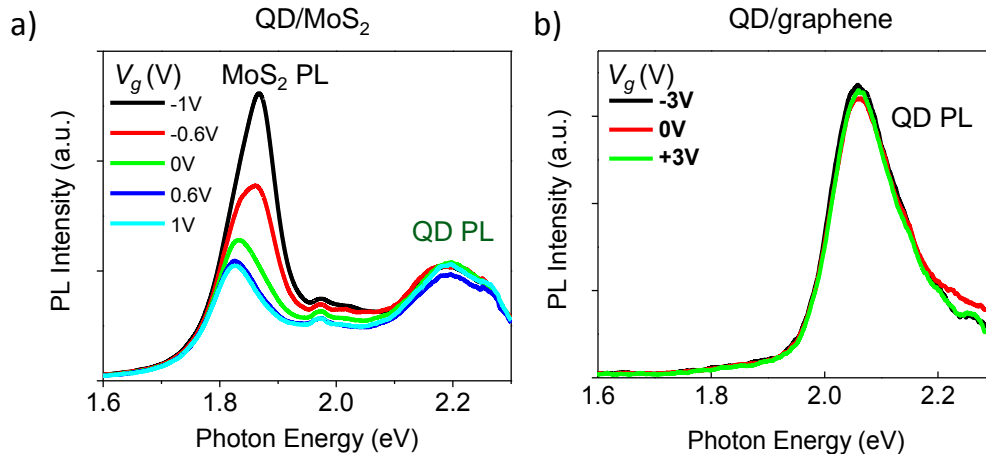
Because of the difference in the intrinsic doping levels, we have to be careful in relating the experimentally measured α_{MoS_2} to the analysis of QD/MoS₂ devices. For $V_g > 0$, the Fermi level of MoS₂ in both MoS₂-only and QD/MoS₂ devices is in the conduction band and the absorption of MoS₂ in both devices changes similarly. On the other hand, when $V_g < 0$, the Fermi level of MoS₂ in MoS₂-only devices is shifted below the conduction band edge. In that case, the density of free carriers and hence α_{MoS_2} are nearly V_g -independent (Fig. S6b). At the same time, the absorption of MoS₂ in QD/MoS₂ devices strongly changes with V_g . This means α_{MoS_2} in QD/MoS₂ and MoS₂-only devices are only close when $V_g > 0$. Because of that, the data in Fig. 4c of the main text are only plotted in that range.

For completeness, we show $Q(\alpha)$ for the entire range from -2V to 2V in the Figure S6c. The discussion above shows that the deviation from linear dependence for $V_g < 0$ is caused by inaccuracy in measured MoS₂ absorption in that voltage range.



Supplementary Figure S6 (a) Photoluminescence spectra of two different MoS₂-only devices without QDs, and of two different QD/MoS₂ devices. (b) Proposed Fermi level (E_F) positioning of MoS₂ in MoS₂-only and QD/MoS₂ devices. (c) $Q(\alpha)$ plot including the data for $V_g < 0$.

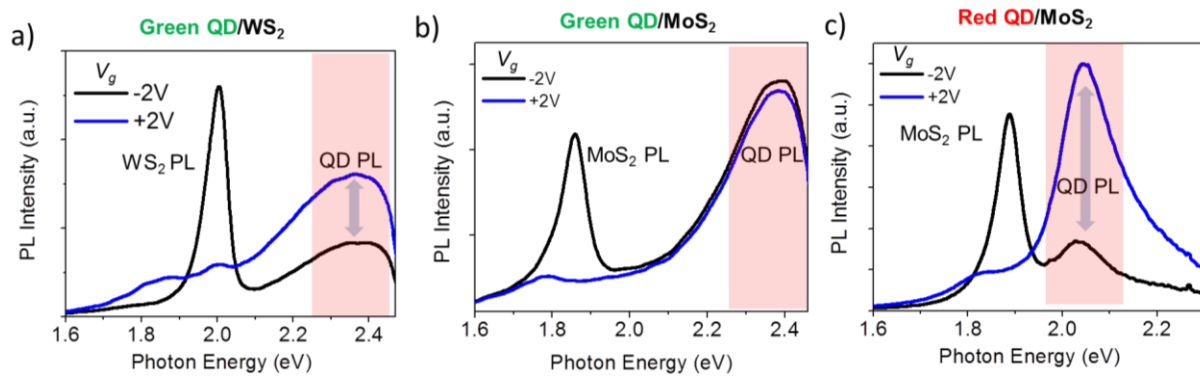
S7. Off-peak QD/MoS₂ and QD/Graphene Devices



Supplementary Figure S7 To check possible contribution of charge transfer to QD PL modulation in QD/MoS₂, two additional types of devices were fabricated. In the first type of device (a) we used CdSSe QD with the emission peak at ~2.2eV (away from the excitonic absorption peak of MoS₂) to make hybrid QD/MoS₂ devices. In the second type of device (b), same QDs as in the rest of the manuscript (emission peak at 2.02eV) were used, but MoS₂ was substituted by monolayer graphene. In both devices, optical absorption of the 2D material was constant at relevant QD emission energies. PL spectra were recorded while varying the gate voltage V_g for both (a)

QD/MoS₂ and (b) QD/graphene devices. In both cases, we observed no changes in the PL at the emission wavelength of the QDs (2.2 eV in (a) and 2.02eV in (b)). This indicates that electrical modulation of the PL for the QDs used in the manuscript is due to changes in excitonic absorption of MoS₂ and not just due to changes in its carrier density.

S8. Spectrally selective tuning of QDs using WS₂ and MoS₂



Supplementary Figure S8. (a) QD/WS₂ devices with QDs emitting at ~2.4eV (green color). The emission peak of these QDs **is** in resonance with excitonic absorption peak of WS₂ (b) QD/MoS₂ devices with QDs emitting at ~2.4eV (green color). The emission peak of these QDs **is not** in resonance with MoS₂ excitonic absorption peak (c) QD/MoS₂ devices with QDs emitting at ~2.02eV (red color). The emission peak of these QDs **is** in resonance with MoS₂ excitonic absorption.